

Magneto-optical magnetometry of individual 30nm cobalt nanowires grown by electron beam induced deposition

E. Nikulina, O. Idigoras, P. Vavassori, A. Chuvilin, and A. Berger

Citation: *Appl. Phys. Lett.* **100**, 142401 (2012); doi: 10.1063/1.3701153

View online: <http://dx.doi.org/10.1063/1.3701153>

View Table of Contents: <http://apl.aip.org/resource/1/APPLAB/v100/i14>

Published by the [American Institute of Physics](http://www.aip.org).

Related Articles

High Faraday effect of antiferromagnetic/ion-crystal photonic crystals in far infrared region
J. Appl. Phys. **113**, 023501 (2013)

Room-temperature sign reversed spin accumulation signals in silicon-based devices using an atomically smooth Fe₃Si/Si(111) contact
J. Appl. Phys. **113**, 013916 (2013)

Investigation of induced Pt magnetic polarization in Pt/Y₃Fe₅O₁₂ bilayers
Appl. Phys. Lett. **101**, 262407 (2012)

Quantitative analysis of electric field induced change in anisotropy field in Co₆₀Fe₂₀B₂₀/(011) xPb(Mg_{1/3}Nb_{2/3})O₃-(1-x)PbTiO₃ (x = 0.68) heterostructures
Appl. Phys. Lett. **101**, 202404 (2012)

Magnetic properties of the magnetophotonic crystal based on bismuth iron garnet
J. Appl. Phys. **112**, 093910 (2012)

Additional information on *Appl. Phys. Lett.*

Journal Homepage: <http://apl.aip.org/>

Journal Information: http://apl.aip.org/about/about_the_journal

Top downloads: http://apl.aip.org/features/most_downloaded

Information for Authors: <http://apl.aip.org/authors>

ADVERTISEMENT

AIP | Applied Physics
Letters

EXPLORE WHAT'S NEW IN APL

SUBMIT YOUR PAPER NOW!

SURFACES AND INTERFACES
Focusing on physical, chemical, biological, structural, optical, magnetic and electrical properties of surfaces and interfaces, and more...

ENERGY CONVERSION AND STORAGE
Focusing on all aspects of static and dynamic energy conversion, energy storage, photovoltaics, solar fuels, batteries, capacitors, thermoelectrics, and more...

Labels in diagram: 1µm-thick LPCVD Silicon Dioxide, Source, Drain, Metal Vias, Ground Ring, QDs, C₆₀, C₇₀, C₈₂, C₈₄, C₈₆, C₈₈, C₉₀, C₉₂, C₉₄, C₉₆, C₉₈, C₁₀₀, C₁₀₂, C₁₀₄, C₁₀₆, C₁₀₈, C₁₁₀, C₁₁₂, C₁₁₄, C₁₁₆, C₁₂₀, C₁₂₆, C₁₃₂, C₁₅₀, C₁₈₀, C₂₄₀, C₃₀₀, C₃₆₀, C₄₂₀, C₄₈₀, C₅₄₀, C₆₀₀, C₆₆₀, C₇₂₀, C₇₈₀, C₈₄₀, C₉₀₀, C₉₆₀, C₁₀₂₀, C₁₀₈₀, C₁₁₄₀, C₁₂₀₀, C₁₂₆₀, C₁₃₂₀, C₁₃₈₀, C₁₄₄₀, C₁₅₀₀, C₁₅₆₀, C₁₆₂₀, C₁₆₈₀, C₁₇₄₀, C₁₈₀₀, C₁₈₆₀, C₁₉₂₀, C₁₉₈₀, C₂₀₄₀, C₂₁₀₀, C₂₁₆₀, C₂₂₂₀, C₂₂₈₀, C₂₃₄₀, C₂₄₀₀, C₂₄₆₀, C₂₅₂₀, C₂₅₈₀, C₂₆₄₀, C₂₇₀₀, C₂₇₆₀, C₂₈₂₀, C₂₈₈₀, C₂₉₄₀, C₃₀₀₀, C₃₀₆₀, C₃₁₂₀, C₃₁₈₀, C₃₂₄₀, C₃₃₀₀, C₃₃₆₀, C₃₄₂₀, C₃₄₈₀, C₃₅₄₀, C₃₆₀₀, C₃₆₆₀, C₃₇₂₀, C₃₇₈₀, C₃₈₄₀, C₃₉₀₀, C₃₉₆₀, C₄₀₂₀, C₄₀₈₀, C₄₁₄₀, C₄₂₀₀, C₄₂₆₀, C₄₃₂₀, C₄₃₈₀, C₄₄₄₀, C₄₅₀₀, C₄₅₆₀, C₄₆₂₀, C₄₆₈₀, C₄₇₄₀, C₄₈₀₀, C₄₈₆₀, C₄₉₂₀, C₄₉₈₀, C₅₀₄₀, C₅₁₀₀, C₅₁₆₀, C₅₂₂₀, C₅₂₈₀, C₅₃₄₀, C₅₄₀₀, C₅₄₆₀, C₅₅₂₀, C₅₅₈₀, C₅₆₄₀, C₅₇₀₀, C₅₇₆₀, C₅₈₂₀, C₅₈₈₀, C₅₉₄₀, C₆₀₀₀, C₆₀₆₀, C₆₁₂₀, C₆₁₈₀, C₆₂₄₀, C₆₃₀₀, C₆₃₆₀, C₆₄₂₀, C₆₄₈₀, C₆₅₄₀, C₆₆₀₀, C₆₆₆₀, C₆₇₂₀, C₆₇₈₀, C₆₈₄₀, C₆₉₀₀, C₆₉₆₀, C₇₀₂₀, C₇₀₈₀, C₇₁₄₀, C₇₂₀₀, C₇₂₆₀, C₇₃₂₀, C₇₃₈₀, C₇₄₄₀, C₇₅₀₀, C₇₅₆₀, C₇₆₂₀, C₇₆₈₀, C₇₇₄₀, C₇₈₀₀, C₇₈₆₀, C₇₉₂₀, C₇₉₈₀, C₈₀₄₀, C₈₁₀₀, C₈₁₆₀, C₈₂₂₀, C₈₂₈₀, C₈₃₄₀, C₈₄₀₀, C₈₄₆₀, C₈₅₂₀, C₈₅₈₀, C₈₆₄₀, C₈₇₀₀, C₈₇₆₀, C₈₈₂₀, C₈₈₈₀, C₈₉₄₀, C₉₀₀₀, C₉₀₆₀, C₉₁₂₀, C₉₁₈₀, C₉₂₄₀, C₉₃₀₀, C₉₃₆₀, C₉₄₂₀, C₉₄₈₀, C₉₅₄₀, C₉₆₀₀, C₉₆₆₀, C₉₇₂₀, C₉₇₈₀, C₉₈₄₀, C₉₉₀₀, C₉₉₆₀, C₁₀₀₂₀, C₁₀₀₈₀, C₁₀₁₄₀, C₁₀₂₀₀, C₁₀₂₆₀, C₁₀₃₂₀, C₁₀₃₈₀, C₁₀₄₄₀, C₁₀₅₀₀, C₁₀₅₆₀, C₁₀₆₂₀, C₁₀₆₈₀, C₁₀₇₄₀, C₁₀₈₀₀, C₁₀₈₆₀, C₁₀₉₂₀, C₁₀₉₈₀, C₁₁₀₄₀, C₁₁₁₀₀, C₁₁₁₆₀, C₁₁₂₂₀, C₁₁₂₈₀, C₁₁₃₄₀, C₁₁₄₀₀, C₁₁₄₆₀, C₁₁₅₂₀, C₁₁₅₈₀, C₁₁₆₄₀, C₁₁₇₀₀, C₁₁₇₆₀, C₁₁₈₂₀, C₁₁₈₈₀, C₁₁₉₄₀, C₁₂₀₀₀, C₁₂₀₆₀, C₁₂₁₂₀, C₁₂₁₈₀, C₁₂₂₄₀, C₁₂₃₀₀, C₁₂₃₆₀, C₁₂₄₂₀, C₁₂₄₈₀, C₁₂₅₄₀, C₁₂₆₀₀, C₁₂₆₆₀, C₁₂₇₂₀, C₁₂₇₈₀, C₁₂₈₄₀, C₁₂₉₀₀, C₁₂₉₆₀, C₁₃₀₂₀, C₁₃₀₈₀, C₁₃₁₄₀, C₁₃₂₀₀, C₁₃₂₆₀, C₁₃₃₂₀, C₁₃₃₈₀, C₁₃₄₄₀, C₁₃₅₀₀, C₁₃₅₆₀, C₁₃₆₂₀, C₁₃₆₈₀, C₁₃₇₄₀, C₁₃₈₀₀, C₁₃₈₆₀, C₁₃₉₂₀, C₁₃₉₈₀, C₁₄₀₄₀, C₁₄₁₀₀, C₁₄₁₆₀, C₁₄₂₂₀, C₁₄₂₈₀, C₁₄₃₄₀, C₁₄₄₀₀, C₁₄₄₆₀, C₁₄₅₂₀, C₁₄₅₈₀, C₁₄₆₄₀, C₁₄₇₀₀, C₁₄₇₆₀, C₁₄₈₂₀, C₁₄₈₈₀, C₁₄₉₄₀, C₁₅₀₀₀, C₁₅₀₆₀, C₁₅₁₂₀, C₁₅₁₈₀, C₁₅₂₄₀, C₁₅₃₀₀, C₁₅₃₆₀, C₁₅₄₂₀, C₁₅₄₈₀, C₁₅₅₄₀, C₁₅₆₀₀, C₁₅₆₆₀, C₁₅₇₂₀, C₁₅₇₈₀, C₁₅₈₄₀, C₁₅₉₀₀, C₁₅₉₆₀, C₁₆₀₂₀, C₁₆₀₈₀, C₁₆₁₄₀, C₁₆₂₀₀, C₁₆₂₆₀, C₁₆₃₂₀, C₁₆₃₈₀, C₁₆₄₄₀, C₁₆₅₀₀, C₁₆₅₆₀, C₁₆₆₂₀, C₁₆₆₈₀, C₁₆₇₄₀, C₁₆₈₀₀, C₁₆₈₆₀, C₁₆₉₂₀, C₁₆₉₈₀, C₁₇₀₄₀, C₁₇₁₀₀, C₁₇₁₆₀, C₁₇₂₂₀, C₁₇₂₈₀, C₁₇₃₄₀, C₁₇₄₀₀, C₁₇₄₆₀, C₁₇₅₂₀, C₁₇₅₈₀, C₁₇₆₄₀, C₁₇₇₀₀, C₁₇₇₆₀, C₁₇₈₂₀, C₁₇₈₈₀, C₁₇₉₄₀, C₁₈₀₀₀, C₁₈₀₆₀, C₁₈₁₂₀, C₁₈₁₈₀, C₁₈₂₄₀, C₁₈₃₀₀, C₁₈₃₆₀, C₁₈₄₂₀, C₁₈₄₈₀, C₁₈₅₄₀, C₁₈₆₀₀, C₁₈₆₆₀, C₁₈₇₂₀, C₁₈₇₈₀, C₁₈₈₄₀, C₁₈₉₀₀, C₁₈₉₆₀, C₁₉₀₂₀, C₁₉₀₈₀, C₁₉₁₄₀, C₁₉₂₀₀, C₁₉₂₆₀, C₁₉₃₂₀, C₁₉₃₈₀, C₁₉₄₄₀, C₁₉₅₀₀, C₁₉₅₆₀, C₁₉₆₂₀, C₁₉₆₈₀, C₁₉₇₄₀, C₁₉₈₀₀, C₁₉₈₆₀, C₁₉₉₂₀, C₁₉₉₈₀, C₂₀₀₄₀, C₂₀₁₀₀, C₂₀₁₆₀, C₂₀₂₂₀, C₂₀₂₈₀, C₂₀₃₄₀, C₂₀₄₀₀, C₂₀₄₆₀, C₂₀₅₂₀, C₂₀₅₈₀, C₂₀₆₄₀, C₂₀₇₀₀, C₂₀₇₆₀, C₂₀₈₂₀, C₂₀₈₈₀, C₂₀₉₄₀, C₂₁₀₀₀, C₂₁₀₆₀, C₂₁₁₂₀, C₂₁₁₈₀, C₂₁₂₄₀, C₂₁₃₀₀, C₂₁₃₆₀, C₂₁₄₂₀, C₂₁₄₈₀, C₂₁₅₄₀, C₂₁₆₀₀, C₂₁₆₆₀, C₂₁₇₂₀, C₂₁₇₈₀, C₂₁₈₄₀, C₂₁₉₀₀, C₂₁₉₆₀, C₂₂₀₂₀, C₂₂₀₈₀, C₂₂₁₄₀, C₂₂₂₀₀, C₂₂₂₆₀, C₂₂₃₂₀, C₂₂₃₈₀, C₂₂₄₄₀, C₂₂₅₀₀, C₂₂₅₆₀, C₂₂₆₂₀, C₂₂₆₈₀, C₂₂₇₄₀, C₂₂₈₀₀, C₂₂₈₆₀, C₂₂₉₂₀, C₂₂₉₈₀, C₂₃₀₄₀, C₂₃₁₀₀, C₂₃₁₆₀, C₂₃₂₂₀, C₂₃₂₈₀, C₂₃₃₄₀, C₂₃₄₀₀, C₂₃₄₆₀, C₂₃₅₂₀, C₂₃₅₈₀, C₂₃₆₄₀, C₂₃₇₀₀, C₂₃₇₆₀, C₂₃₈₂₀, C₂₃₈₈₀, C₂₃₉₄₀, C₂₄₀₀₀, C₂₄₀₆₀, C₂₄₁₂₀, C₂₄₁₈₀, C₂₄₂₄₀, C₂₄₃₀₀, C₂₄₃₆₀, C₂₄₄₂₀, C₂₄₄₈₀, C₂₄₅₄₀, C₂₄₆₀₀, C₂₄₆₆₀, C₂₄₇₂₀, C₂₄₇₈₀, C₂₄₈₄₀, C₂₄₉₀₀, C₂₄₉₆₀, C₂₅₀₂₀, C₂₅₀₈₀, C₂₅₁₄₀, C₂₅₂₀₀, C₂₅₂₆₀, C₂₅₃₂₀, C₂₅₃₈₀, C₂₅₄₄₀, C₂₅₅₀₀, C₂₅₅₆₀, C₂₅₆₂₀, C₂₅₆₈₀, C₂₅₇₄₀, C₂₅₈₀₀, C₂₅₈₆₀, C₂₅₉₂₀, C₂₅₉₈₀, C₂₆₀₄₀, C₂₆₁₀₀, C₂₆₁₆₀, C₂₆₂₂₀, C₂₆₂₈₀, C₂₆₃₄₀, C₂₆₄₀₀, C₂₆₄₆₀, C₂₆₅₂₀, C₂₆₅₈₀, C₂₆₆₄₀, C₂₆₇₀₀, C₂₆₇₆₀, C₂₆₈₂₀, C₂₆₈₈₀, C₂₆₉₄₀, C₂₇₀₀₀, C₂₇₀₆₀, C₂₇₁₂₀, C₂₇₁₈₀, C₂₇₂₄₀, C₂₇₃₀₀, C₂₇₃₆₀, C₂₇₄₂₀, C₂₇₄₈₀, C₂₇₅₄₀, C₂₇₆₀₀, C₂₇₆₆₀, C₂₇₇₂₀, C₂₇₇₈₀, C₂₇₈₄₀, C₂₇₉₀₀, C₂₇₉₆₀, C₂₈₀₂₀, C₂₈₀₈₀, C₂₈₁₄₀, C₂₈₂₀₀, C₂₈₂₆₀, C₂₈₃₂₀, C₂₈₃₈₀, C₂₈₄₄₀, C₂₈₅₀₀, C₂₈₅₆₀, C₂₈₆₂₀, C₂₈₆₈₀, C₂₈₇₄₀, C₂₈₈₀₀, C₂₈₈₆₀, C₂₈₉₂₀, C₂₈₉₈₀, C₂₉₀₄₀, C₂₉₁₀₀, C₂₉₁₆₀, C₂₉₂₂₀, C₂₉₂₈₀, C₂₉₃₄₀, C₂₉₄₀₀, C₂₉₄₆₀, C₂₉₅₂₀, C₂₉₅₈₀, C₂₉₆₄₀, C₂₉₇₀₀, C₂₉₇₆₀, C₂₉₈₂₀, C₂₉₈₈₀, C₂₉₉₄₀, C₂₉₉₈₀, C₃₀₀₄₀, C₃₀₁₀₀, C₃₀₁₆₀, C₃₀₂₂₀, C₃₀₂₈₀, C₃₀₃₄₀, C₃₀₄₀₀, C₃₀₄₆₀, C₃₀₅₂₀, C₃₀₅₈₀, C₃₀₆₄₀, C₃₀₇₀₀, C₃₀₇₆₀, C₃₀₈₂₀, C₃₀₈₈₀, C₃₀₉₄₀, C₃₁₀₀₀, C₃₁₀₆₀, C₃₁₁₂₀, C₃₁₁₈₀, C₃₁₂₄₀, C₃₁₃₀₀, C₃₁₃₆₀, C₃₁₄₂₀, C₃₁₄₈₀, C₃₁₅₄₀, C₃₁₆₀₀, C₃₁₆₆₀, C₃₁₇₂₀, C₃₁₇₈₀, C₃₁₈₄₀, C₃₁₉₀₀, C₃₁₉₆₀, C₃₂₀₂₀, C₃₂₀₈₀, C₃₂₁₄₀, C₃₂₂₀₀, C₃₂₂₆₀, C₃₂₃₂₀, C₃₂₃₈₀, C₃₂₄₄₀, C₃₂₅₀₀, C₃₂₅₆₀, C₃₂₆₂₀, C₃₂₆₈₀, C₃₂₇₄₀, C₃₂₈₀₀, C₃₂₈₆₀, C₃₂₉₂₀, C₃₂₉₈₀, C₃₃₀₄₀, C₃₃₁₀₀, C₃₃₁₆₀, C₃₃₂₂₀, C₃₃₂₈₀, C₃₃₃₄₀, C₃₃₄₀₀, C₃₃₄₆₀, C₃₃₅₂₀, C₃₃₅₈₀, C₃₃₆₄₀, C₃₃₇₀₀, C₃₃₇₆₀, C₃₃₈₂₀, C₃₃₈₈₀, C₃₃₉₄₀, C₃₄₀₀₀, C₃₄₀₆₀, C₃₄₁₂₀, C₃₄₁₈₀, C₃₄₂₄₀, C₃₄₃₀₀, C₃₄₃₆₀, C₃₄₄₂₀, C₃₄₄₈₀, C₃₄₅₄₀, C₃₄₆₀₀, C₃₄₆₆₀, C₃₄₇₂₀, C₃₄₇₈₀, C₃₄₈₄₀, C₃₄₉₀₀, C₃₄₉₆₀, C₃₅₀₂₀, C₃₅₀₈₀, C₃₅₁₄₀, C₃₅₂₀₀, C₃₅₂₆₀, C₃₅₃₂₀, C₃₅₃₈₀, C₃₅₄₄₀, C₃₅₅₀₀, C₃₅₅₆₀, C₃₅₆₂₀, C₃₅₆₈₀, C₃₅₇₄₀, C₃₅₈₀₀, C₃₅₈₆₀, C₃₅₉₂₀, C₃₅₉₈₀, C₃₆₀₄₀, C₃₆₁₀₀, C₃₆₁₆₀, C₃₆₂₂₀, C₃₆₂₈₀, C₃₆₃₄₀, C₃₆₄₀₀, C₃₆₄₆₀, C₃₆₅₂₀, C₃₆₅₈₀, C₃₆₆₄₀, C₃₆₇₀₀, C₃₆₇₆₀, C₃₆₈₂₀, C₃₆₈₈₀, C₃₆₉₄₀, C₃₇₀₀₀, C₃₇₀₆₀, C₃₇₁₂₀, C₃₇₁₈₀, C₃₇₂₄₀, C₃₇₃₀₀, C₃₇₃₆₀, C₃₇₄₂₀, C₃₇₄₈₀, C₃₇₅₄₀, C₃₇₆₀₀, C₃₇₆₆₀, C₃₇₇₂₀, C₃₇₇₈₀, C₃₇₈₄₀, C₃₇₉₀₀, C₃₇₉₆₀, C₃₈₀₂₀, C₃₈₀₈₀, C₃₈₁₄₀, C₃₈₂₀₀, C₃₈₂₆₀, C₃₈₃₂₀, C₃₈₃₈₀, C₃₈₄₄₀, C₃₈₅₀₀, C₃₈₅₆₀, C₃₈₆₂₀, C₃₈₆₈₀, C₃₈₇₄₀, C₃₈₈₀₀, C₃₈₈₆₀, C₃₈₉₂₀, C₃₈₉₈₀, C₃₉₀₄₀, C₃₉₁₀₀, C₃₉₁₆₀, C₃₉₂₂₀, C₃₉₂₈₀, C₃₉₃₄₀, C₃₉₄₀₀, C₃₉₄₆₀, C₃₉₅₂₀, C₃₉₅₈₀, C₃₉₆₄₀, C₃₉₇₀₀, C₃₉₇₆₀, C₃₉₈₂₀, C₃₉₈₈₀, C₃₉₉₄₀, C₃₉₉₈₀, C₄₀₀₄₀, C₄₀₁₀₀, C₄₀₁₆₀, C₄₀₂₂₀, C₄₀₂₈₀, C₄₀₃₄₀, C₄₀₄₀₀, C₄₀₄₆₀, C₄₀₅₂₀, C₄₀₅₈₀, C₄₀₆₄₀, C₄₀₇₀₀, C₄₀₇₆₀, C₄₀₈₂₀, C₄₀₈₈₀, C₄₀₉₄₀, C₄₁₀₀₀, C₄₁₀₆₀, C₄₁₁₂₀, C₄₁₁₈₀, C₄₁₂₄₀, C₄₁₃₀₀, C₄₁₃₆₀, C₄₁₄₂₀, C₄₁₄₈₀, C₄₁₅₄₀, C₄₁₆₀₀, C₄₁₆₆₀, C₄₁₇₂₀, C₄₁₇₈₀, C₄₁₈₄₀, C₄₁₉₀₀, C₄₁₉₆₀, C₄₂₀₂₀, C₄₂₀₈₀, C₄₂₁₄₀, C₄₂₂₀₀, C₄₂₂₆₀, C₄₂₃₂₀, C₄₂₃₈₀, C₄₂₄₄₀, C₄₂₅₀₀, C₄₂₅₆₀, C₄₂₆₂₀, C₄₂₆₈₀, C₄₂₇₄₀, C₄₂₈₀₀, C₄₂₈₆₀, C₄₂₉₂₀, C₄₂₉₈₀, C₄₃₀₄₀, C₄₃₁₀₀, C₄₃₁₆₀, C₄₃₂₂₀, C₄₃₂₈₀, C₄₃₃₄₀, C₄₃₄₀₀, C₄₃₄₆₀, C₄₃₅₂₀, C₄₃₅₈₀, C₄₃₆₄₀, C₄₃₇₀₀, C₄₃₇₆₀, C₄₃₈₂₀, C₄₃₈₈₀, C₄₃₉₄₀, C₄₄₀₀₀, C₄₄₀₆₀, C₄₄₁₂₀, C₄₄₁₈₀, C₄₄₂₄₀, C₄₄₃₀₀, C₄₄₃₆₀, C₄₄₄₂₀, C₄₄₄₈₀, C₄₄₅₄₀, C₄₄₆₀₀, C₄₄₆₆₀, C₄₄₇₂₀, C₄₄₇₈₀, C₄₄₈₄₀, C₄₄₉₀₀, C₄₄₉₆₀, C₄₅₀₂₀, C₄₅₀₈₀, C₄₅₁₄₀, C₄₅₂₀₀, C₄₅₂₆₀, C₄₅₃₂₀, C₄₅₃₈₀, C₄₅₄₄₀, C₄₅₅₀₀, C₄₅₅₆₀, C₄₅₆₂₀, C₄₅₆₈₀, C₄₅₇₄₀, C₄₅₈₀₀, C₄₅₈₆₀, C₄₅₉₂₀, C₄₅₉₈₀, C₄₆₀₄₀, C₄₆₁₀₀, C₄₆₁₆₀, C₄₆₂₂₀, C₄₆₂₈₀, C₄₆₃₄₀, C₄₆₄₀₀, C₄₆₄₆₀, C₄₆₅₂₀, C₄₆₅₈₀, C₄₆₆₄₀, C₄₆₇₀₀, C₄₆₇₆₀, C₄₆₈₂₀, C₄₆₈₈₀, C₄₆₉₄₀, C₄₇₀₀₀, C₄₇₀₆₀, C₄₇₁₂₀, C₄₇₁₈₀, C₄₇₂₄₀, C₄₇₃₀₀, C₄₇₃₆₀, C₄₇₄₂₀, C₄₇₄₈₀, C₄₇₅₄₀, C₄₇₆₀₀, C₄₇₆₆₀, C₄₇₇₂₀, C₄₇₇₈₀, C₄₇₈₄₀, C₄₇₉₀₀, C₄₇₉₆₀, C₄₈₀₂₀, C₄₈₀₈₀, C₄₈₁₄₀, C₄₈₂₀₀, C₄₈₂₆₀, C₄₈₃₂₀, C₄₈₃₈₀, C₄₈₄₄₀, C₄₈₅₀₀, C₄₈₅₆₀, C₄₈₆₂₀, C₄₈₆₈₀, C₄₈₇₄₀, C₄₈₈₀₀, C₄₈₈₆₀, C₄₈₉₂₀, C₄₈₉₈₀, C₄₉₀₄₀, C₄₉₁₀₀, C₄₉₁₆₀, C₄₉₂₂₀, C₄₉₂₈₀, C₄₉₃₄₀, C₄₉₄₀₀, C₄₉₄₆₀, C₄₉₅₂₀, C₄₉₅₈₀, C₄₉₆₄₀, C₄₉₇₀₀, C₄₉₇₆₀, C₄₉₈₂₀, C₄₉₈₈₀, C₄₉₉₄₀, C₄₉₉₈₀, C₅₀₀₄₀, C₅₀₁₀₀, C₅₀₁₆₀, C₅₀₂₂₀, C₅₀₂₈₀, C₅₀₃₄₀, C₅₀₄₀₀, C₅₀₄₆₀, C₅₀₅₂₀, C₅₀₅₈₀, C₅₀₆₄₀, C₅₀₇₀₀, C₅₀₇₆₀, C₅₀₈₂₀, C₅₀₈₈₀, C₅₀₉₄₀, C₅₁₀₀₀, C₅₁₀₆₀, C₅₁₁₂₀, C₅₁₁₈₀, C₅₁₂₄₀, C₅₁₃₀₀, C₅₁₃₆₀, C₅₁₄₂₀, C₅₁₄₈₀, C₅₁₅₄₀, C₅₁₆₀₀, C₅₁₆₆₀, C₅₁₇₂₀, C₅₁₇₈₀, C₅₁₈₄₀, C₅₁₉₀₀, C₅₁₉₆₀, C₅₂₀₂₀, C₅₂₀₈₀, C₅₂₁₄₀, C₅₂₂₀₀, C₅₂₂₆₀, C₅₂₃₂₀, C₅₂₃₈₀, C₅₂₄₄₀, C₅₂₅₀₀, C₅₂₅₆₀, C₅₂₆₂₀, C₅₂₆₈₀, C₅₂₇₄₀, C₅₂₈₀₀, C₅₂₈₆₀, C₅₂₉₂₀, C₅₂₉₈₀, C₅₃₀₄₀, C₅₃₁₀₀, C₅₃₁₆₀, C₅₃₂₂₀, C₅₃₂₈₀, C₅₃₃₄₀, C₅₃₄₀₀, C₅₃₄₆₀, C₅₃₅₂₀, C₅

Magneto-optical magnetometry of individual 30 nm cobalt nanowires grown by electron beam induced deposition

E. Nikulina,^{1,a)} O. Idigoras,¹ P. Vavassori,^{1,2} A. Chuvilin,^{1,2} and A. Berger¹

¹CIC NanoGUNE Consolider, Tolosa Hiribidea 76, 20018 Donostia-San Sebastian, Spain

²Ikerbasque, Basque Foundation for Science, Alameda Urquijo 36-5, 48011 Bilbao, Spain

(Received 25 January 2012; accepted 18 March 2012; published online 2 April 2012)

We show that magnetometry measurements based upon the magneto-optical Kerr effect and high resolution optical microscopy can be used as a noninvasive probe of magnetization reversal for individual nano-structures. Our measurements demonstrate single pass hysteresis loop measurements for sample sizes down to 30 nm width. A quantitative signal-to-noise ratio evaluation shows that our approach achieves an at least 3-fold improvement in sensitivity if compared to focused laser based nano-magnetometry. An analysis of the physical limits of our detection scheme enables us to estimate that measurements for structures with single digit nm widths and magnetic moments of 10^{-16} Am² are feasible. © 2012 American Institute of Physics. [<http://dx.doi.org/10.1063/1.3701153>]

Miniaturization of ferromagnetic elements is a key thrust area in the field of magnetism and relevant for a wide range of applications, such as magnetic devices for high-density storage,¹ magnetic field sensors,^{2,3} biosensors,⁴ and logic elements.⁵ Continuous advances in nanofabrication technology are, therefore, pushing the dimension of ferromagnetic structures into the realm of the extreme nanoscale regime. Besides well-established multi-step lithography techniques being commonly used for the fabrication of magnetic nanostructures, an alternative has been proposed and developed during the last years by facilitating electron beam induced deposition (EBID).^{2,3,6-9} This technique is a potentially very attractive alternative at least for some nanotechnology aspects, such as rapid prototyping, because it is a one-step technique and, thus, relatively simple, flexible, and fast. Also, it has the potential of engineering and fabricating extremely small structures, even below the 1 nm length scale.¹⁰

In EBID, an electron beam is used to decompose an appropriate precursor gas into its volatile and nonvolatile components, as shown in Fig. 1. The nonvolatile component then forms a deposit of predefined size and shape on the substrate. An example can be seen as the inset of Fig. 1. For most materials, however, it has been found to be a most challenging task to fabricate even moderately pure, small structures by this EBID method. Nonetheless, it has already been shown that EBID allows the growth of cobalt magnetic structures with an exceptionally high purity of up to 95 atomic percent (at. %) of cobalt.⁹ Regarding the deposition resolution, lateral sizes down to 30 nm have recently been demonstrated by using low beam currents and adjusted precursor flux.¹¹ In the same work,¹¹ it was shown by means of electron holography, that such 30 nm wide Co wires are indeed ferromagnetic. However, due to the limitations of applying and freely modifying magnetic fields inside an electron microscope, more comprehensive studies of the magnetism in these wires were not possible.

Although microscopic probes capable of imaging magnetic states in ultrasmall structures have been developed, such as Lorentz microscopy,¹² electron holography,^{12,13} and scanning electron microscopy with polarization analysis,¹⁴ and are thus capable of detecting magnetism in very small volumes, they are generally not compatible with the application of relevant magnetic field sequences for the study of magnetic responses or magnetization reversal. While this limitation is less severe for other magnetic microscopy techniques, such as spin-polarized tunnel microscopy (spin-STM)¹⁵ or magnetic force microscopy and related resonance techniques,¹⁶ there are other limiting boundary conditions such as the *in situ* preparation requirement for spin-STMs, for instance, which severely limit their broad utilization. There are other highly advanced magnetometry techniques that have been demonstrated to be sufficiently sensitive for nano-scale magnets, such as Hall-probe based techniques as well as micro- and nano-SQUIDs.¹⁷ Unfortunately, these techniques, while having excellent sensitivities, require the fabrication of specialized samples and are, therefore, neither flexible nor compatible with general samples and sample shapes. Nonetheless, it is most desirable to study the magnetization reversal of *individual* ultrasmall structures and have a general, flexible, and non-destructive tool to do so. Arrays of

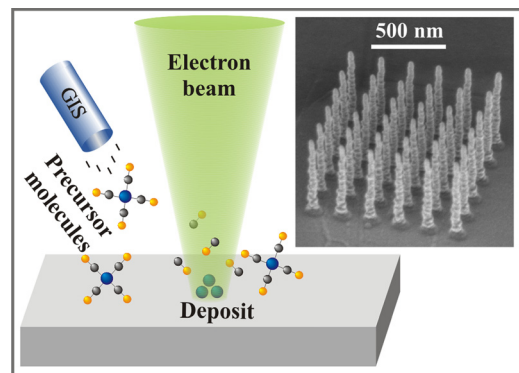


FIG. 1. (a) Schematics of the EBID process; the inset shows a scanning electron microscopy image of a cobalt pillar array fabricated by EBID.

^{a)}Electronic mail: e.nikulina@nanogune.eu.

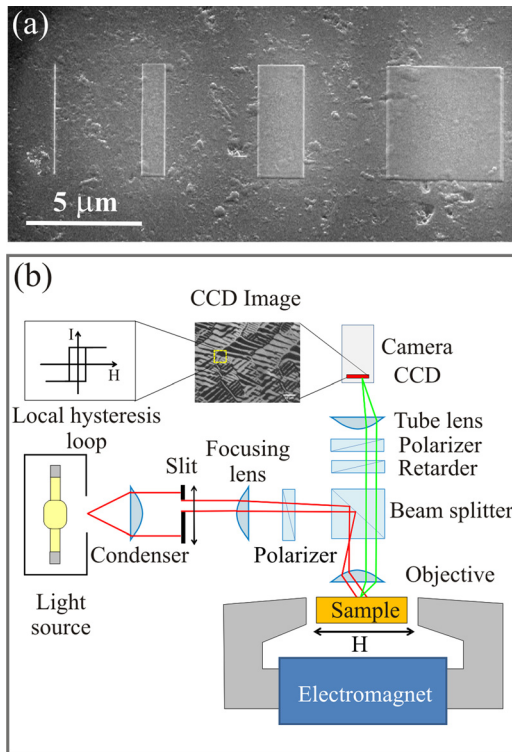


FIG. 2. (a) Scanning electron microscopy image showing the set of EBID cobalt structures, referred to as set 1 in Table I. (b) Schematic sketch of the MOKE microscope utilized in this study, including the two operation modes that it enables: magnetic domain imaging²⁴ and local high resolution magnetometry.

many nanostructures, which collectively are magnetic entities that are large enough for more conventional magnetometry techniques, represent a serious limitation due to statistical averaging and smoothing out of results caused by unavoidable fabrication variability, defects, and interactions within such structures.

In this paper, we report the fabrication of high purity, ultrasmall Co nanostructures with lateral dimension down to 30 nm and the measurement of their magnetic properties by means of magneto-optical Kerr effect (MOKE) magnetometry, utilizing a MOKE microscope for the measurement of *single shot* hysteresis loops of *individual* ultrasmall nanomagnets. This experimental achievement represents a substantially improved sensitivity with respect to focused laser based MOKE nano-magnetometry setups, which have been employed so far for such studies.^{18–22} Our results demonstrate that the combination of EBID and MOKE microscopy makes it possible to explore the magnetization reversal of *individual* ultrasmall magnetic nanostructures with lateral dimension down to the 30 nm length scale and below and, thus, opens up a broadly applicable avenue to perform systematic research on individual nano-scale magnets.

The electron beam induced deposition of cobalt was performed in a Helios NanoLabTM DualBeamTM (FEI, Netherlands) equipped with a Schottky field-emission electron gun and an integrated gas injection system (GIS). For the fabrication process, the following parameters were used: background vacuum = $2 \cdot 10^{-4}$ Pa, precursor gas pressure = $8 \cdot 10^{-4}$ Pa, dwell time = 1 μ s, pitch = 5 nm, and sample to GIS-tube distance = 50 μ m. While a large number of different structures were fabricated and studied, we focus here on three specific sets of cobalt structures, for which experimental results are presented. Each set consists of four structures with the same length of 5 μ m and different widths of 5 μ m, 2 μ m, 1 μ m and the minimum 1 pixel line for deposition. A SEM picture of one of these sample sets is shown in Fig. 2(a), while Table I lists key parameters for all three sets, namely: the deposition conditions, the SEM verified dimensions for the smallest structure in each set, as well as the atomic composition as measured by energy-dispersive x-ray spectrometry (EDX) for test structures grown under identical conditions. The dimensions listed in Table I demonstrate that with the appropriate deposition conditions, we were able to create wire structures down to 30 nm width. This particular structure is visible on the left hand side of Fig. 2(a).

Previous studies of the magnetization reversal of individual sub-micron wires made use of MOKE systems based on focused cw laser beams.^{18–22} The sensitivity of a given MOKE setup can be defined as the minimum fractional signal $(\Delta I/I_0)_{\min}$ detectable with a signal-to-noise (S/N) ratio of 2, where $\Delta I = I(M) - I(-M)$ is the MOKE signal variation upon reversal of magnetization and $I_0 = [I(M) + I(-M)]/2$ is the average light intensity signal. While the fractional MOKE signal $\Delta I/I_0$ for a continuous film does not depend on the illuminated area, the MOKE signal amplitude ΔI is diluted in the case of individual sub-wavelength magnets according to the aspect ratio (AR) of the magnet area to the total illuminated area. Commonly, focused laser beams are hereby utilized in order to increase AR, and thus $(\Delta I/I_0)_{\min}$, as much as possible. The smallest nanostructure measured in a single sweep hysteresis loop with $S/N = 2$ that is reported in the literature is an individual 200 nm wide and 5 nm thick Permalloy nanowire.²² This represents a single sweep measurement sensitivity of approximately 6×10^{-15} Am² (the length of the illuminated structure was about 5 μ m). A noise analysis shows that for measurement systems based on focused laser beams and for a material like Permalloy (Kerr rotation angle $\theta_k \sim 3 \mu$ rad), the maximum S/N that is theoretically reachable in a single shot measurement of $\Delta I/I_0$ is $(S/N)_{\max} \approx 2$, using the highest laser power available without causing significant heating of the sample.²² Therefore, this previously reported measurement has practically achieved the theoretical performance limit reachable by means of the focused laser MOKE nano-magnetometry approach. In order

TABLE I. Deposition conditions, corresponding compositions, and dimensions of EBID grown cobalt structures.

	Deposition conditions	Content in at. %	Dimensions of the thinnest line (L × H × W)
Set 1	30 kV, 2.7 nA, 60 min	Co:C:O = 82:12:6	5 μ m × 20 nm × 30 nm
Set 2	2 kV, 2.7 nA, 3 min	Co:C:O = 82:13:5	5 μ m × 7.5 nm × 55 nm
Set 3	2 kV, 2.7 nA, 30 min	Co:C:O = 82:13:5	5 μ m × 75 nm × 115 nm

to push beyond this present limitation in MOKE nano-magnetometry performance, we pursued a different approach: we have utilized an optical wide-field polarization microscope optimized for Kerr microscopy (Evico Magnetics GmbH, Germany). The microscope is equipped with an electromagnet that allows the application of a magnetic field of up to 500 mT along an arbitrary direction in the sample plane and with a high sensitivity CCD camera that is capable of taking magnetic-contrast images of the sample surface with a spatial resolution of the order of 500 nm. The key feature of our approach is that we can measure the field dependent local magnetization, i.e., a local hysteresis loop, by selecting an arbitrary (shape, size, and position in the field of view) region of interest (ROI), by means of a reduced number of pixels within the CCD camera array, and use it as a conventional light intensity detector. A schematic of the Kerr microscope setup and its operation mode for magnetometry is shown in Fig. 2(b). Thanks to this feature, we can maximize AR well beyond what is achievable by using focused laser techniques. This is especially relevant for high aspect ratio nanostructures, such as wires, for which we can keep the value of AR close to 1 and thus about 2 orders of magnitude higher than what is achievable with focused laser beams for truly nano-sized objects. The advantage of keeping AR as high as possible is evident from the measurement reported in Fig. 3(b), where we show that we are able to record a single shot hysteresis loop with an average S/N of 4.1 per data point for a 20 nm thick Co wire that is only 30 nm wide using a ROI of 340×8 pixels corresponding to $AR \approx 0.25$ (at the optical magnification that we used here, an individual CCD pixel corresponds to an area of $15 \times 15 \text{ nm}^2$ on the sample surface), as schematically shown in Fig. 3(a). Renormalized to the $S/N = 2$ criterion, this represents a single sweep measurement sensitivity of $2 \times 10^{-15} \text{ Am}^2$, which corresponds to a 3-fold improvement over the previously reported sensitivity using focused laser based MOKE magnetometry.^{18–22} Our achievement is further confirmed by single sweep loop measurements with $S/N = 4.4$ on a 7.5 nm thick Co wire of 55 nm width, shown in Fig. 3(c), which corresponds to a sensitivity of $1.0 \times 10^{-15} \text{ Am}^2$. Also in this case, we used the same ROI of 340×8 pixels corresponding now to an $AR \approx 0.5$. The achievement of a slightly higher S/N for the wider wire, in spite of the reduction of the magnetic volume by a factor of about 1.5, confirms that maximization of the AR is the key factor underlying the improved performance of our approach. These sensitivity figures also compare very favorably with the sensitivity of 10^{-12} to 10^{-13} Am^2 for the latest generation of SQUID magnetometer. It is worth to point out that we have not reached the fundamental limit in our micro-MOKE sensitivity performance. To a good approximation, the S/N scales with the square root of the light intensity I per unit of area that is used to illuminate the sample, which in the present study is $1 \mu\text{W}/\mu\text{m}^2$, about 100 times smaller than that typically used in focused beams systems. Therefore, by simply increasing I by 100 times, which is technically feasible, we should be able to gain an additional order of magnitude in sensitivity down to $1 \times 10^{-16} \text{ Am}^2$ without causing significant heating of the sample. Our experimental achievement also implies that even substantially narrower and/or shorter Co nano-

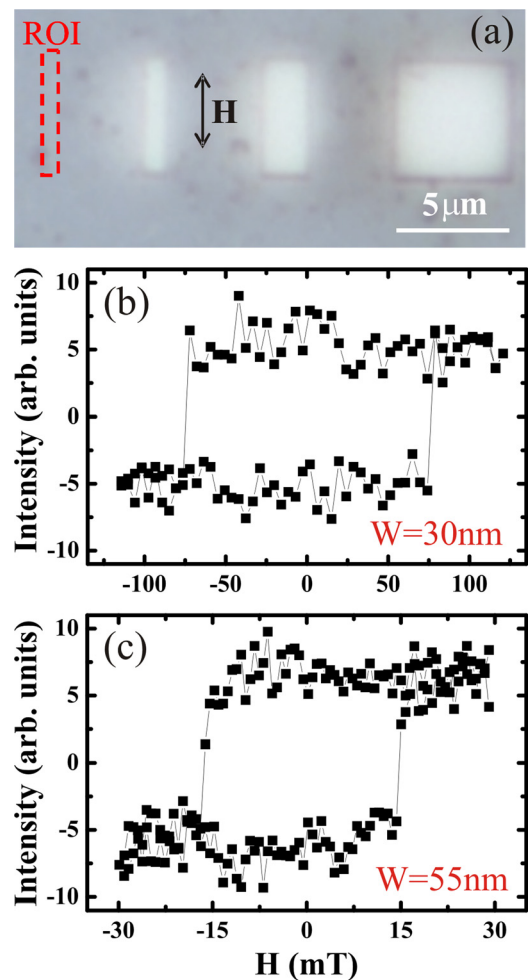


FIG. 3. (a) Optical microscope image of the set 1 cobalt EBID structures, as acquired by the MOKE enabled microscope; the red dashed frame shows schematically the ROI selected to enclose the thinnest cobalt line, which is only 30 nm wide and barely visible here. (b) Single shot MOKE hysteresis loop signal using a ROI as indicated in panel (a) for the $W = 30 \text{ nm}$ wide wire. (c) Same as in panel (b), but for the $W = 55 \text{ nm}$ wide wire.

structures could be measured in this way by averaging multiple hysteresis loop sequences. In Fig. 4, we compare hysteresis loops measured on single isolated Co wires of different widths and thicknesses (see Table I). A SEM image of each wire is shown next to the corresponding hysteresis loop. The magnetic field was applied in the plane of the sample, parallel to the long axis of the wires. Each hysteresis loop shown in this figure is the average of 9 single shot measurements. For the cases displayed in Figs. 4(a) and 4(b), namely, the 30 nm and 55 nm wide Co wires discussed above, we find that upon averaging 9 loops the S/N has increased by a factor of close to 3 as expected. This confirms that a wire of less than 10 nm width could be studied by means of our magneto-optical approach. The remarkably square loop shape measured for our two narrow wires is expected, given that the external field is applied along the wire length, which is the easy axis of magnetization due to shape anisotropy. We observed coercive field values of 75, 15.5, and 5.5 mT for 30, 55, and 115 nm wire widths, respectively. The reduction of the field values triggering the magnetization reversal as the wire width increases is consistent with the magnetization reversal being induced by the nucleation of domain

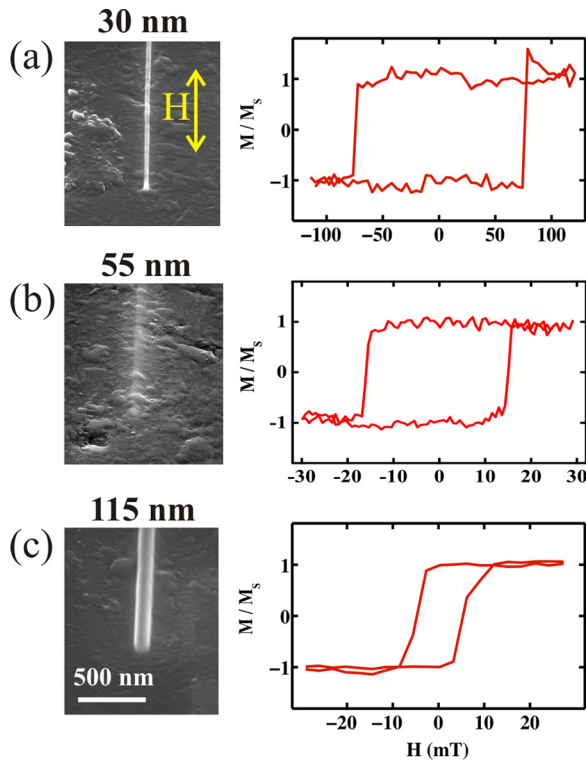


FIG. 4. Scanning electron microscopy images of cobalt nanowires with widths of 30 nm (a), 55 nm (b), and 115 nm (c) and the corresponding magnetization hysteresis loops as determined by means of MOKE magnetometry. Each loop is an average of 9 measurements.

walls at wire ends and their subsequent abrupt displacement along the wire.²³ Interestingly, the loop obtained for the 115 nm wide wire also shows a smaller second feature as it approaches saturation at 11 mT. This fact indicates that this wire's magnetization reversal is more complex, as one would expect due to its larger cross section area, which enables meta-stable or even stable non-uniform magnetization configurations to form near the end points. This type of fine structure is often lost in large arrays, because its specific characteristics will depend crucially on fine details of the nano-scale geometry. This in turn highlights the importance of studying magnetic properties such as magnetization reversal on individual nano-elements and reinforces the need and value of characterization methods that have this capability, such as the one we have demonstrated here.

We acknowledge the financial support from FEI Company (Netherlands), the Basque Government under the Etorrek Program contract No. IE11-304, as well as the Spanish Ministry of Science and Education under Project No. MAT2009-07980. O.I. acknowledges the Basque Government for the Formación de Investigadores fellowships No. BFI09.284.

- ¹C. Chappert, A. Fert, and F. N. Van Dau, *Nature Mater.* **6**, 813 (2007).
- ²G. Boero, I. Utke, T. Bret, N. Quack, M. Todorova, S. Mouaziz, P. Kejik, J. Brugger, R. S. Popovic, and P. Hoffmann, *Appl. Phys. Lett.* **86**, 042503 (2005).
- ³M. Gabureac, L. Bernau, I. Utke, and G. Boero, *Nanotechnology* **21**, 115503 (2010).
- ⁴V. C. Martins, J. Germano, F. A. Cardoso, J. Loureiro, S. Cardoso, L. Sousa, M. Piedade, L. P. Fonseca, and P. P. Freitas, *J. Magn. Magn. Mater.* **322**, 1655 (2010).
- ⁵D. A. Allwood, G. Xiong, C. C. Faulkner, D. Atkinson, D. Petit, and R. P. Cowburn, *Science* **309**, 1688 (2005).
- ⁶I. Utke, P. Hoffmann, and J. Melngailis, *J. Vac. Sci. Technol. B* **26**, 1197 (2008).
- ⁷Y. M. Lau, P. C. Chee, J. T. L. Thong, and V. Ng, *J. Vac. Sci. Technol. A* **20**, 1295 (2002).
- ⁸I. Utke, V. Friedli, J. Michler, T. Bret, X. Multone, and P. Hoffmann, *Appl. Phys. Lett.* **88**, 031906 (2006).
- ⁹A. Fernández-Pacheco, J. M. De Teresa, R. Córdoba, and M. R. Ibarra, *J. Phys. D: Appl. Phys.* **42**, 055005 (2009).
- ¹⁰W. F. van Dorp, B. van Someren, C. W. Hagen, and P. Kruit, *Nano Lett.* **5**, 1303 (2005).
- ¹¹L. Serrano-Ramón, R. Córdoba, L. A. Rodríguez, C. Magén, E. Snoeck, C. Gatel, I. Serrano, M. R. Ibarra, and J. M. De Teresa, *ACS Nano* **5**, 7781 (2011).
- ¹²J. N. Chapman, *J. Phys. D: Appl. Phys.* **17**, 623 (1984).
- ¹³H. Lichte and M. Lehmann, *Rep. Prog. Phys.* **71**, 016102 (2008).
- ¹⁴S. Hankemeier, A. Kobs, R. Frömter, and H. P. Oepen, *Phys. Rev. B* **82**, 064414 (2010).
- ¹⁵S. Krause, G. Herzog, T. Stapelfeldt, L. Berbil-Bautista, M. Bode, E. Y. Vedmedenko, and R. Wiesendanger, *Phys. Rev. Lett.* **103**, 127202 (2009).
- ¹⁶J. P. Davis, D. Vick, D. C. Fortin, J. A. J. Burgess, W. K. Hiebert, and M. R. Freeman, *Appl. Phys. Lett.* **96**, 072513 (2010).
- ¹⁷W. Wernsdorfer, *Supercond. Sci. Technol.* **22**, 064013 (2009).
- ¹⁸R. P. Cowburn, D. K. Koltsov, A. O. Adeyeye, and M. E. Welland, *Appl. Phys. Lett.* **73**, 3947 (1998).
- ¹⁹D. Atkinson, D. A. Allwood, G. Xiong, M. D. Cooke, C. C. Faulkner, and R. P. Cowburn, *Nature Mater.* **2**, 85 (2003).
- ²⁰E. Puppin, P. Vavassori, and L. Callegaro, *Rev. Sci. Instrum.* **71**, 1752 (2000).
- ²¹G. Gubbiotti, S. Tacchi, G. Carlotti, P. Vavassori, N. Singh, S. Goolaup, A. O. Adeyeye, A. Stashkevich, and M. Kostylev, *Phys. Rev. B* **72**, 224413 (2005).
- ²²D. A. Allwood, G. Xiong, M. D. Cooke, and R. P. Cowburn, *J. Phys. D: Appl. Phys.* **36**, 2175 (2003).
- ²³M. Grimsditch, A. Berger, J. Johnson, V. Metlushko, B. Ilic, P. Neuzil, and R. Kumar, *Europhys. Lett.* **54**, 813 (2001).
- ²⁴O. Idigoras, P. Vavassori, J. M. Porro, and A. Berger, *J. Magn. Magn. Mater.* **320**, L57–L60 (2010).